ELSEVIER

Chemical Geology 172 (2000) 113–130

CHEMICAL GEOLOGY
INCLUDING
ISOTOPE GEOSCIENCE

www.elsevier.com/locate/chemgeo

Monazite U–Pb and Th–Pb geochronology by ion microprobe, with an application to in situ dating of an Archean metasedimentary rock

Richard A. Stern [a,*], Robert G. Berman [b]

[a] *J.C. Roddick Ion Microprobe Laboratory, Geological Survey of Canada, 601 Booth Street, Ottawa, ONT, Canada K1A 0E8*
[b] *Continental Geoscience Division, Geological Survey of Canada, 615 Booth Street, Ottawa, ONT, Canada K1A 0E8*

Abstract

Monazite grains from nine different Precambrian rock samples and having concordant isotope dilution U–Pb and Th–Pb ages were used to develop and evaluate techniques for U–Pb, Th–Pb, and Pb–Pb isotopic dating using an ion microprobe operating at high mass resolution ($R = 5500$, 1%). An unidentified isobar at ~ 203.960 amu complicated the determination of ^{204}Pb in the monazites with higher Th, but it appeared to have been eliminated when using a slight energy offset. The $^{207}Pb^*/^{206}Pb^*$ ratios of individual spots were determined in 10 min analyses to ± 0.3–0.5% (1σ) of the true values using a 20-μm-wide O_2^- primary beam, whereas the uncertainty in the mean of several spots on a single generation of monazite was typically ± 0.1–0.4% (2σ). Instrumental bias in the measured Pb^+/UO^+ and Pb^+/ThO^+ values of individual analyses was monitored using linear relationships between $^{206}Pb^+/UO^+$ vs. UO_2^+/UO^+ and $^{208}Pb^+/ThO^+$ vs. UO_2^+/UO^+. The bias appears to vary somewhat with monazite Th content, requiring the use of compositionally matched standards. Individual spot measurements of the $^{206}Pb/^{238}U$ and $^{208}Pb/^{232}Th$ ratios in unknown monazites of low to moderate Th can be determined to $\pm 2\%$ (1σ).

The dating technique was applied to in situ analysis of small monazite inclusions hosted in an amphibolite-grade metapelite of Archean origin. Both the contextual setting and the morphology of the monazite grains were found to be important factors in interpreting the timing of growth of the host metamorphic mineral (e.g., garnet, staurolite, plagioclase). Euhedral monazite grains armoured in low-CaO garnet and matrix plagioclase yielded an age of 2548 ± 17 Ma, interpreted as dating an early episode of low-pressure metamorphism. Partially resorbed monazite within a high-CaO garnet rim yielded ages of ca. 2500 Ma, but are interpreted as inherited from the first event rather than syn-genetic with respect to the growth of this garnet. An age of 1755 ± 30 Ma was obtained for anhedral monazite associated with late, chlorite-filled fractures, apparently reflecting post-tectonic retrogression.

Keywords: Monazite U–Pb and Th–Pb geochronology; Ion microprobe; Archean metasedimentary rock

1. Introduction

In the last few years, laboratories equipped with large-radius ion microprobes have been turning their attention increasingly towards determining the Pb–

* Corresponding author.
E-mail address: rstern@nrcan.gc.ca (R.A. Stern).

0009-2541/00/$ - see front matter
PII: S0009-2541(00)00239-4

Pb, U–Pb, and Th–Pb isotopic ages of the mineral monazite [$Ce(La,Th)PO_4$]. The ion microprobe method has wide utility, for example, in determining the crystallization ages of leucogranites (Harrison et al., 1995), in studying monazite diffusion profiles (Grove and Harrison, 1999), in sediment provenance studies (Sircombe and Compston, 1994; Sircombe, 1997), and especially the dating of monazite in metamorphic rocks (e.g., DeWolf et al., 1993; Williams et al., 1996; Vry et al., 1996; Ireland and Gibson, 1998; Zhu and O'Nions, 1999; Zhu et al., 1997a,b). In metamorphic rocks, the capability of the ion microprobe to examine monazite in situ, i.e., in thin-section or rock chip (e.g., Zhu et al., 1997a,b), offers exciting prospects for elucidating the ages of specific mineral assemblages or tectonic fabrics. Our own interest in monazite ion microprobe dating stems from a desire to understand the metamorphic history recorded within amphibolite-grade metasedimentary rocks from an Archean greenstone terrain of northern Canada. Specifically, we saw an opportunity to place age constraints on the pressure and temperature estimates determined from the mineral phase equilibria through the in situ dating of tiny monazite inclusions.

When this study began in 1996, there was little published information about the methodology of ion microprobe dating of monazite and certainly no widely available monazite reference materials. Consequently, an investigation was initiated into monazite geochronology using our Sensitive High (mass) Resolution Ion Microprobe (SHRIMP II), founded upon a suite of monazites with concordant isotope dilution U–Pb and Th–Pb ages (Stern and Sanborn, 1998). Our current methodology is summarized here, with information on the nature and mitigation of two particular analytical problems, firstly, the presence of isobaric interferences on ^{204}Pb despite the use of high mass resolution (Williams et al., 1996; Sircombe, 1997; Stern and Sanborn, 1998; Ireland and Gibson, 1998), and, secondly, on potentially significant matrix effects on the Pb–U and Pb–Th calibrations (Stern and Sanborn, 1998; Zhu et al., 1998). In the final part of the report, we illustrate the utility of the methodology with an example application to in situ dating of the aforementioned monazites within an Archean metapelitic rock. Here, knowledge of the spatial context of the grains as well as their morphological attributes provide important additional constraints on the interpretation of the isotopic ages.

2. Experimental design

The study was divided into two parts. In part 1, Precambrian igneous and metamorphic monazite grains from nine different rocks were examined using the SHRIMP ion microprobe in three separate grain mounts. This stage of the study was designed to work out the analytical protocols and to test for suitably homogenous samples that could become reference materials. The particular populations of monazite grains were originally selected based on their high degree of concordance with respect to the isotope dilution–thermal ionization mass spectrometry (ID–TIMS) U–Pb and Th–Pb data acquired in our laboratory. We did not acquire both SHRIMP and ID–TIMS data from identical grains.

In part 2 of the study, SHRIMP U–Pb ages were acquired in situ for monazites exposed on polished chips of a garnet metapelite of presumed Archean age.

3. Instrumentation and techniques

For grain mounts, the selected monazites were arranged upon double-sided tape within a 25 mm diameter × 7 mm deep Teflon™ mould. Araldite resin was then poured into the mould and allowed to harden at 40°C overnight. The mounts were polished with diamond compound (9, 6, and 1 μm) to reveal the grain centers. The mounts were then washed with a soap solution, rinsed in deionized water, and photographed in reflected and transmitted plane light. The mounts were washed again with soap and deionized water, and dried under a heat lamp at 40°C. The cleaned mounts were coated evaporatively with 5.8–6.0 nm of Au (99.9999%). Following coating, backscattered electron (BSE) images were obtained using a scanning electron microscope (SEM). We found that the samples displayed no contrast using a broad-band cathodoluminescence detector. The samples were subsequently placed within a steel holder and surface conductivity measured, generally 10–20

Ω/cm. The mounts were then placed within the sample vacuum lock of the ion microprobe for a minimum of 12 h prior to quantitative analysis.

For the in situ work in this study, centimeter-size blocks of the rock sample were arranged within the usual 25-mm mould, and grains of standard monazite placed in between. Subsequent sample preparation was identical to that described above, with the exception that a 10–12 nm layer of Au was required for optimum conductivity. Study of polished thin sections is also routine, but requires special procedures for the embedding of monazite standards into the thin section.

The study employed the SHRIMP II at the Geological Survey of Canada (Stern, 1996, 1997). Detailed descriptions of the SHRIMP II instrument may be found elsewhere (e.g., Stern, 1997; Williams, 1998; De Laeter and Kennedy, 1998). In brief, primary oxygen ions generated in a duoplasmatron by gas discharge in a hollow Ni cathode are accelerated through 10 kV, mass-filtered, and projected onto the target using Kohler ion imaging (see Williams, 1998). The O_2^- primary ion species was used in this study, with sputtering occurring from flat-bottomed elliptical spots measuring about 20 μm in the long dimension during the testing phase, and 5 μm for the in situ study. Primary ion currents were respectively 1–2 nA and ~100 pA. Secondary ion accelerating voltage is nominally 10 kV, with the first extraction electrode at 750 V with respect to the sample surface. The source slit and collector slit widths were set at 100 and 90 μm, respectively, giving an operating mass resolution (1% peak height) of 5500–5700, with flat top peaks 0.012–0.013 amu wide.

The width of the post-electrostatic analyzer (ESA) window was set at 2.5 mm, equivalent to an energy bandwidth of 20 eV. No energy offsets were employed (cf. Harrison et al., 1995; Zhu et al., 1998) except where specified in the text for testing purposes. For the acquisition of energy scans, i.e., ion energy vs. ion count rate profiles, a slit of 100 μm width, equivalent to an energy bandpass of 0.8 eV, was manually traversed across the energy spectrum on the ESA focal plane in 100–200 μm steps. Ion arrival rates are measured using a single electron multiplier coupled with an ion counting system. Deadtime for the system has been measured using Pb standards at 25 ns. Overall instrumental Pb sensitivity for monazite is estimated to be 30–35 cps/ppm/nA using primary O_2^-.

Table 1
Mass stations and count times for a typical monazite analysis

Mass station	Isotope	Mass (amu)	Typical count time (s)	Delay for magnetic settling (s)
1	$^{203}CePO_2$	202.869	2	2
2	^{204}Pb	203.973	20	1
3	background	204.100	20	1
4	^{206}Pb	205.974	10	1
5	^{207}Pb	206.976	25	1
6	^{208}Pb	207.977	3	1
7	^{248}ThO	248.033	3	1
8	^{254}UO	254.046	5	1
9	$^{270}UO_2$	270.041	5	1

The sample preparation procedure and conductive Au coating contribute measurable common Pb to the surface of the mount. The surface Pb contamination was eliminated prior to a quantitative analysis by rastering the primary beam for 3 min over an area slightly larger than the analysis pit. An isotopic analysis comprised five to eight sequential visits of the required masses (Table 1). The study used the 'snapshot' technique, whereby the isotopic composition and error is determined from mid-point of the analysis period (Williams, 1998; Stern, 1997, 1998).

The ID–TIMS data for single grains of monazite were obtained from existing published and unpublished data (referenced in Table 2), supplemented by additional U–Pb and Th–Pb analyses conducted by Davis et al. (1998). In all cases, ID–TIMS analytical methods for monazite U–Pb age determinations followed the methods described in Parrish et al. (1987), whereas the techniques of monazite Th–Pb age determinations and the Th–Pb data used in this study are provided by Davis et al. (1998).

BSE images of the monazites were obtained using a Cambridge Instruments S360 scanning electron microscope operating at 20 kV accelerating potential and using an electron beam current of 2–5 nA.

4. Part I: technique development and standards

Table 2 presents a summary of the ID–TIMS isotopic data for single grains (10–20 μg) of the test

Table 2
Summary of ID–TIMS U–Pb and Th–Pb isotopic ages of single concordant monazite grains. Data as referenced and from Stern and Sanborn (1998) and Davis et al. (1998)

Monazite sample (rock type, reference)	$^{207}Pb/^{206}Pb$ age (Ma, $\pm 2\sigma$)	$^{232}Th/^{208}Pb$ age (Ma, $\pm 2\sigma$)	Mean U (ppm, 1s)	Mean Th (wt. %, 1s)	Best age estimate (Ma)	Best $^{207}Pb/^{206}Pb$ estimate
High-Th laboratory standard #4170 (monzogranite; Wodicka and Scott, 1997)	1836.0 ± 0.5 ($n = 6$)	1832 ± 11 ($n = 3$)	1068 (183) ($n = 6$)	9.1 (1.1) ($n = 6$)	**1836**	**0.11224**
Medium-Th laboratory standard #3345 (paragneiss; Bethune and Scammell, 1997)	1821.0 ± 0.6 ($n = 5$)	1822 ± 9 ($n = 1$)	3228 (533) ($n = 5$)	7.3 (0.6) ($n = 5$)	**1821**	**0.11132**
Low-Th laboratory standard #2908 (granite; Parrish and Hanmer, unpublished data)	1795.2 ± 0.7 ($n = 5$)	1787 ± 9 ($n = 1$)	2319 (823) ($n = 5$)	2.0 (0.5) ($n = 5$)	**1795**	**0.10973**
#1861 (leucosome; Percival et al., 1992)	2666 ± 1.0 ($n = 3$)	2667 ± 13 ($n = 1$)	2158 (369) ($n = 4$)	4.5 (0.3) ($n = 4$)	2666	0.18143
#1859 (diatexite; Percival et al., 1992)	2662 ± 1 ($n = 3$)	2676 ± 13 ($n = 1$)	752 (48) ($n = 3$)	7.0 (0.7) ($n = 3$)	2662	0.18099
#4323 (syenogranite; Bostock and van Breemen, unpublished data)	1935.1 ± 0.5 ($n = 7$)	1938 ± 9	4597 (2057)	5.3 (2.1)	1935	0.11858
#1409 (pegmatite; Roddick and Bleeker, unpublished data)	1768.4 ± 0.7 ($n = 5$)	1777 ± 9 ($n = 1$)	2124 (356)	12.0 (1.2)	1768	0.10812
#2775 (orthogneiss; Corriveau et al., 1996)	1166 ± 3 ($n = 3$)	1169 ± 6	306 (145)	5.3 (0.8)	1166	0.07876
#2234 (fenite; Hogarth and van Breemen, 1996)	1016 ± 2 ($n = 5$)	1017 ± 5	247 (50)	0.69 (0.14)	1016	0.07307

samples, which have U–Pb and Th–Pb ages ranging from 1.02 to 2.67 Ga. Replicate analyses demonstrate the isotopic homogeneity of most of the samples, and the concordance of the U–Pb and Th–Pb isotopic systems.

In discussing the analytical methods, the following conventions apply: a '$^{+}$' sign indicates a raw count rate or isotopic ratio (e.g., $^{204}Pb^{+}$), the use of '*' indicates that the Pb isotope has been corrected for common Pb (e.g., $^{206}Pb^{*}$), and where no signs are present (e.g., $^{206}Pb/^{238}U$), it is assumed that all corrections have been applied. The designation for one standard deviation is '1s', and 95% confidence intervals are indicated by '2σ'. Decay constants used in age calculations are from Steiger and Jäger (1977).

4.1. Pb isotopes

The analysis of the radiogenic Pb isotopes in the test monazites was generally straightforward owing to the relatively high abundances of total radiogenic Pb (thousands of ppm) and low common Pb. Typical uncertainties (1σ) of $^{207}Pb^{+}/^{206}Pb^{+}$ values were ±0.3–0.5% per spot, and 2σ uncertainties of ±0.2% were typical for the mean of numerous spots from the same monazite populations (Stern and Sanborn, 1998). The Pb isotopes were corrected for background count rates monitored at 204.1 amu, which averaged 0.3 ± 0.1 cps/nA primary O_2^-.

In Fig. 1a, the weighted mean $^{207}Pb^{+}/^{206}Pb^{+}$ values for the test samples are plotted as the percentage difference relative to the ID–TIMS values (Table 2) vs. mean $^{204}Pb^{+}/^{206}Pb^{+}$ ratio. The $^{207}Pb^{+}/^{206}Pb^{+}$ values exceed the accepted values by +0.03% to +1.10%, and the deviations are positively correlated with $^{204}Pb^{+}/^{206}Pb^{+}$, a relationship that is consistent with the presence of intrinsic common Pb in the monazites (cf. Sircombe, 1997). For samples with mean $^{204}Pb^{+}/^{206}Pb^{+}$ values < 0.00005, the deviation of $^{207}Pb^{+}/^{206}Pb^{+}$ values from true values is $< +0.11\%$, indicating a high degree

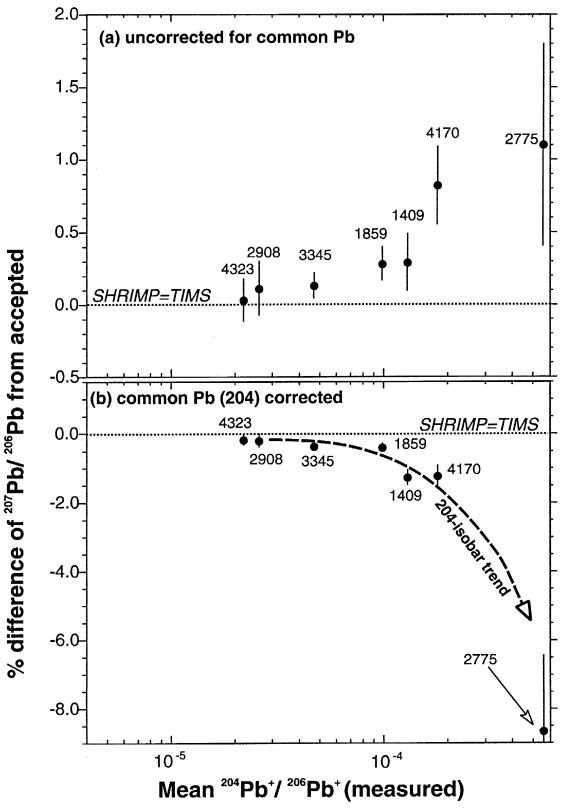

Fig. 1. Percent difference between SHRIMP weighted mean $^{207}Pb/^{206}Pb$ ratios and the accepted values (ID–TIMS, Table 2) vs. $^{204}Pb/^{206}Pb$: (a) raw data, uncorrected for common Pb; (b) corrected for common Pb using measured $^{204+}Pb/^{206+}Pb$ ratios (204-method, see Stern, 1997) and a Cumming and Richards' (1975) model for the common Pb composition. See text for discussion. The $\pm 2\sigma$ uncertainties are shown where larger than symbol.

of accuracy of raw data that are relatively unaffected by common Pb. Due to the effective pre-analysis rastering technique, any common Pb in the analysis must be due entirely to that within the monazite. Accordingly, the $^{207}Pb^{+}/^{206}Pb^{+}$ values were corrected for the presence of common Pb using the measured $^{204}Pb^{+}/^{206}Pb^{+}$ values (204-method) and the Cumming and Richards (1975) model for common Pb composition (see Stern, 1997). Corrected as such (Fig. 1b), however, the test samples have $^{207}Pb^{*}/^{206}Pb^{*}$ values that are less than the accepted values. The deviations from the ID–TIMS values correlate with $^{204}Pb^{+}/^{206}Pb^{+}$, i.e., being relatively small (-0.2%) for samples with $^{204}Pb^{+}/^{206}Pb^{+}$ values of < 0.00005, but up to -8.7% for the sample with highest mean $^{204}Pb^{+}/^{206}Pb^{+}$. The inverse correlation between $^{204}Pb^{+}/^{206}Pb^{+}$ and $^{207}Pb^{*}/^{206}Pb^{*}$ observed in Fig. 1b was also evident when considering data sets for individual test samples, such as shown in Fig. 2b for high Th monazite #4170.

The trends displayed in Figs. 1b and 2b are consistent with an isobaric interference on $^{204}Pb^{+}$. Stern and Sanborn (1998) showed that the intensity of the 204 isobar was related to monazite Th content (Fig. 3). The ID–TIMS data revealed no such systematic relationship between the ^{204}Pb and Th content, i.e., high-Th monazites had the same levels of common Pb as low-Th monazites. Mass scans in the

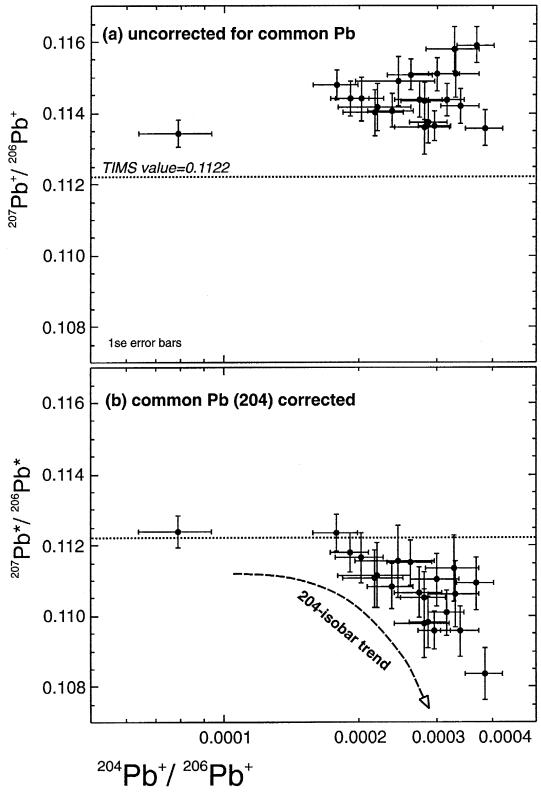

Fig. 2. An example of a data set for a high-Th monazite sample (4170) in which the 204-isobar is quite easily recognized in a plot of $^{204}Pb^{+}/^{206}Pb^{+}$ vs. $^{207}Pb^{+}/^{206}Pb^{+}$. (a) Data uncorrected for common Pb, showing intrinsic common Pb in the monazite analyses. (b) Data corrected for common Pb by the 204-method. The inverse correlation converging on the accepted value is indicative of an isobaric interference on mass 204.

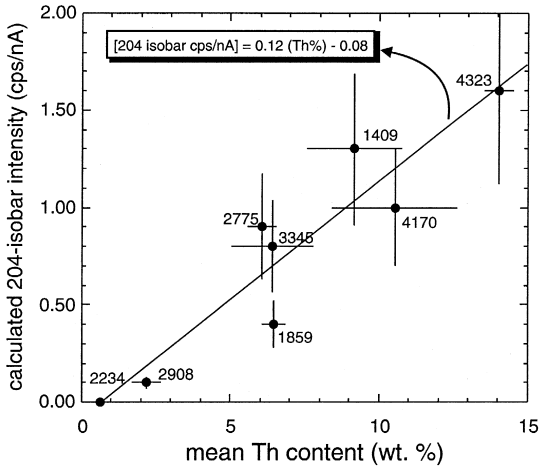

Fig. 3. Mean Th abundance (determined by SHRIMP) vs. intensity of the interfering 204 isobar (in cps/nA), calculated using the difference between the observed and predicted $^{207}Pb/^{206}Pb$ values (see Stern and Sanborn, 1998). The indicated equation was used to estimate the 204 isobar intensity in an unknown analysis.

vicinity of 204 amu confirmed the presence of an isotope at $\sim 203.960 \pm 0.005$ amu (Stern and Sanborn, 1998), which is for all practical purposes irresolvable from ^{204}Pb using the SHRIMP II ion microprobe. The elemental composition of this isotope has not yet been determined, although the experiments below indicate that it is a complex molecular ion. Stern and Sanborn (1998) developed a procedure for correcting for the presence of the 204 isobar based on the Th content of the analyzed monazites, and this procedure was used to correct the data in the second part of this study.

Near the completion of the study, however, it was found that the 204 isobar could be eliminated if the ESA window was adjusted at a central position 2 mm further to the high-energy side of the secondary ion spectrum, equivalent to a shift of $+15$–20 eV. A similar effect could presumably be achieved by adjusting the ESA voltage to a higher value. To what extent, if at all, the 204 corrected Pb-isotope ratios of monazites of unknown isotopic composition have been influenced by the isobar thus depends on the instrumental setup in addition to monazite composition. For data sets of unknown monazites, a negative trend on the type of plot shown in Figs. 1b and 2b would indicate an isobar problem. Only $^{207}Pb^+/^{206}Pb^+$ analyses having $^{204}Pb^+/^{206}Pb^+ > 0.0001$ would be sufficiently affected by the isobar to warrant attention. For Phanerozoic and younger monazites, the proportion of common Pb can be estimated alternatively by correcting the $^{207}Pb^+/^{206}Pb^+$ values to the $^{207}Pb^*/^{206}Pb^*$ at an assumed age (207-method; Ireland and Gibson, 1998).

Stern and Sanborn (1998) estimated fractionation of the Pb isotopes at $< 0.2\%$/amu in monazite based on the difference between the $^{207}Pb^*/^{206}Pb^*$ values measured with the SHRIMP and ID–TIMS, consistent with the $< 0.1\%$/amu value determined in the same fashion by Harrison et al. (1995). Due to the difficulty in accurately measuring the small mass fractionation in monazite, no separate correction was applied to the data in this paper.

4.2. U and Th abundances and Th / U ratios

An estimate of the U content in monazite was obtained from the following relationship (after Stern and Sanborn, 1998):

$$U_{unk} = k\left(UO_2^+/^{203}CePO_2^+\right)$$

where U_{unk} is the U content of the unknown in ppm (weight), $UO_2^+/^{203}CePO_2^+$ is the value measured for the unknown, and 'k' is a constant derived for the particular instrumental setup. The $^{203}CePO_2^+$ isotope is assumed to be at the same concentration level in all the monazites. The constant 'k' is the average value obtained for the test samples, for which ID–TIMS U concentration data are available (Table 1), and had a value of 313 during this study (Stern and Sanborn, 1998). The ratio involving the UO_2^+ isotope was found to be less sensitive to instrumental conditions than either UO^+ or U^+. The uncertainty in the calculated U contents using this method is estimated at no better than $\pm 20\%$.

The Th/U ratios were estimated from the measured ThO^+/UO^+ values, corrected for instrumental fractionation:

$$^{232}Th/^{238}U = f_{ThO-UO}(ThO^+/UO^+)$$

The f_{ThO-UO} value was determined to be 0.857 (Stern and Sanborn, 1998), and is within the 0.835–0.888 range obtained by other SHRIMP workers as well as for the Cameca IMS 1270 (Williams et al., 1996; Harrison et al., 1995; Sircombe, 1997; Ireland

and Gibson, 1998), indicating that the $f_{\mathrm{ThO-UO}}$ is not influenced greatly by the specific instrumentation or analytical conditions. The uncertainty associated with determination of Th/U ratios in monazite is $< \pm 1\%$. Th contents were obtained from the Th/U weight ratio and the U contents.

4.3. $^{206}Pb/^{238}U$ and $^{208}Pb/^{232}Th$

Following Harrison et al. (1995) and Zhu et al. (1998), we found that the intensity vs. energy profiles of the secondary ions from monazite were valuable in developing protocols for determining $^{206}Pb/^{238}U$ and $^{208}Pb/^{232}Th$. An example energy scan carried out upon a high-Th monazite (sample 1409, Table 2) is shown in Fig. 4 on a log-scale plot of ion intensity vs. relative eV. The profiles for $^{208}Pb^+$ and $^{206}Pb^+$ are identical, with narrow maxima (which approximates 10 keV ions) and moderately steep decreases in intensity with increasing kinetic energy. As found by previous workers, the UO_2^+ and ThO_2^+ profiles are very similar to each other and to those of Pb^+. The UO^+ and ThO^+ profiles are also similar to each other, with shallower energy tailing compared with the dioxides and Pb^+. Similarly, the profiles for $^{238}U^+$ and Th^+ are subparallel to each other, having very broad maxima at about +5 eV and very shallow tailing compared with Pb^+. The $^{203}CePO_2^+$ profile is typical of complex molecular ions, with a sharp maximum at 0 eV and steep drop with increasing energy.

If the accelerating potential of the secondary ions varies for any particular reason, such as local sample charging, then variations in the intensity of the Pb^+ isotopes should correlate best with UO_2^+ and ThO_2^+ (e.g., Harrison et al., 1995; Zhu et al., 1998). On this reasoning, Harrison et al. (1995) and Zhu et al. (1997b,1998) utilized the UO_2^+/U^+ and ThO_2^+/Th^+

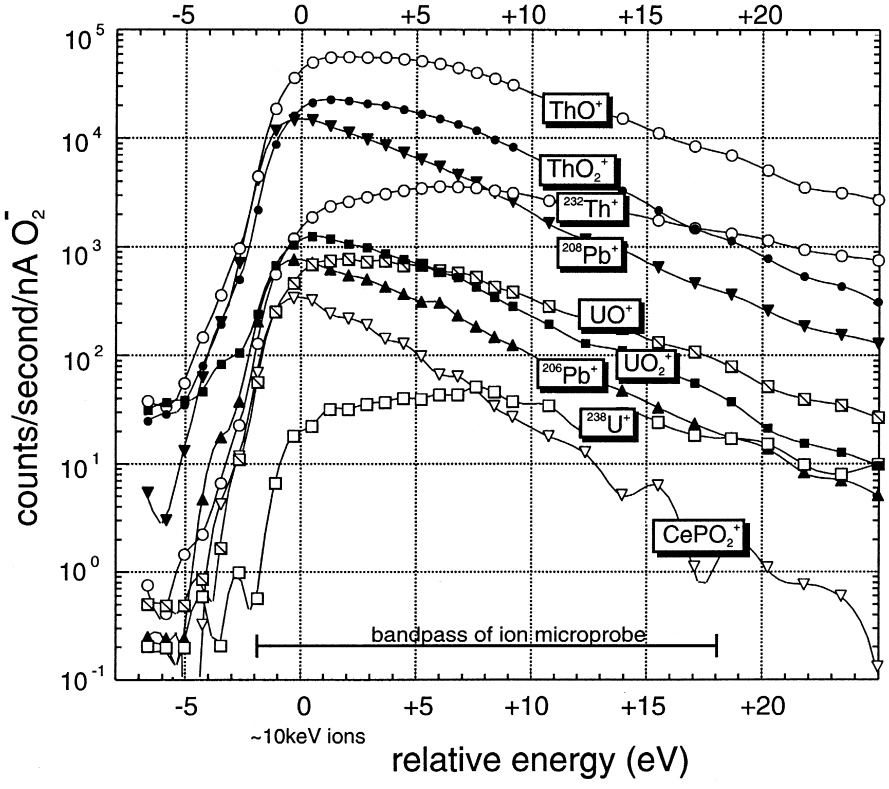

Fig. 4. Plot of relative ion energy vs. intensity for a high-Th monazite (sample 1409, Table 2). Note that although the relative ion energies are well-determined, absolute calibration of ion energy is not possible; instead, it is assumed that the prevalent maxima correspond to an initial kinetic energy of 0 eV.

ratios as monitors of the working conditions during analysis for Pb^+/U^+ and Pb^+/Th^+, respectively. In this study, we utilized the UO_2^+/UO^+ value to monitor spot conditions for calibrating both the Pb^+/UO^+ and Pb^+/ThO^+ ratios. Examples of the Pb–U and Pb–Th correlations, fitted using linear regression, are shown in Fig. 5 for three Paleoproterozoic monazites. Based on their well-behaved Pb/U and Pb/Th calibrations, monazites #4170, #3345, and #2908 (Table 2) were adopted as the in-house calibration standards (Stern and Sanborn, 1998).

The bias-corrected $(^{206}Pb/^{238}U)_{unk}$ and $(^{208}Pb/^{238}Th)_{unk}$ values for an unknown spot are derived

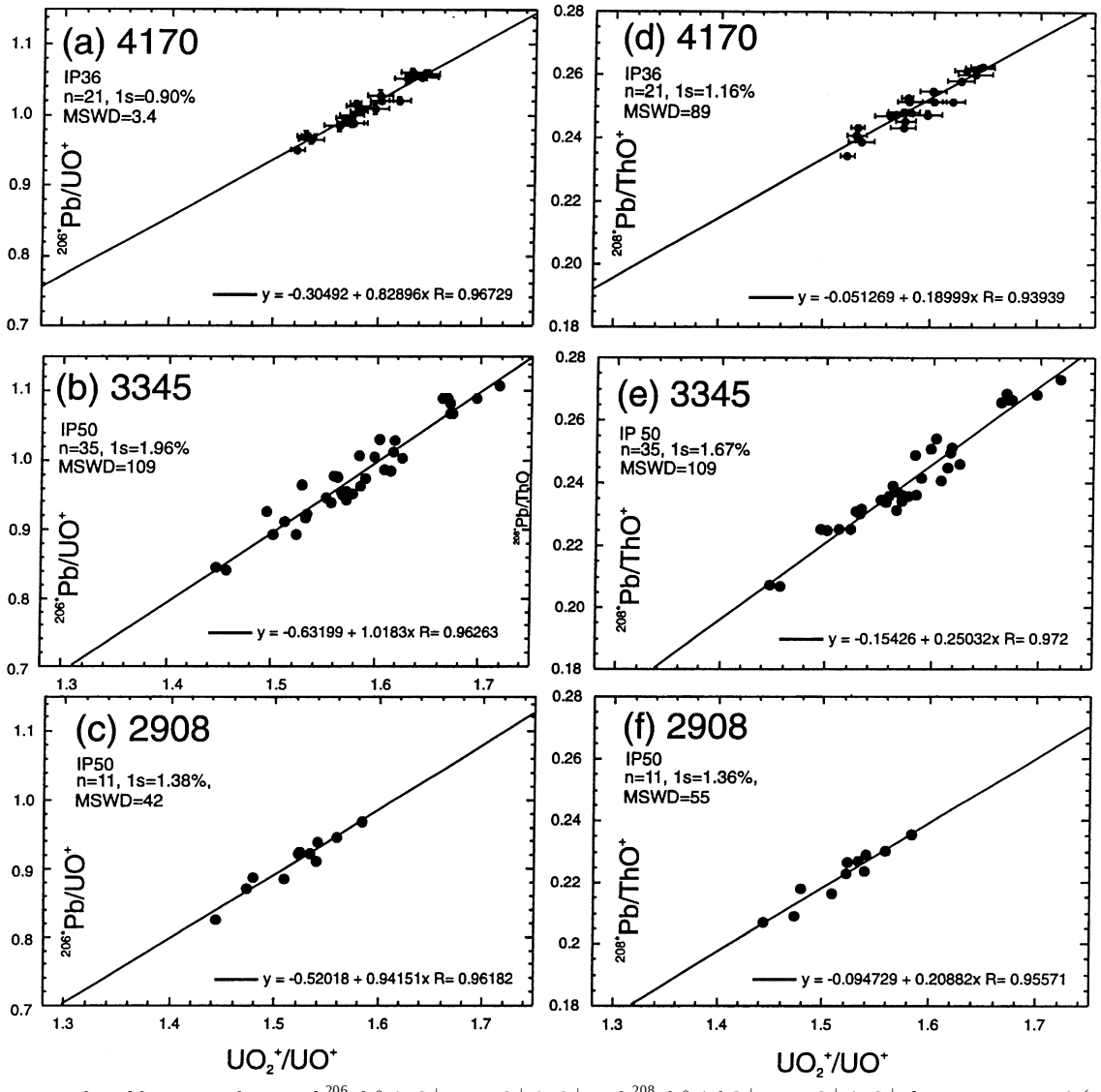

Fig. 5. Examples of linear correlations of $^{206}Pb^*/UO^+$ vs. UO_2^+/UO^+ and $^{208}Pb^*/ThO^+$ vs. UO_2^+/UO^+ for monazites 4170 (a, d), 3345 (b, e), and 2908 (c, f), now adopted as in-house monazite standards (Table 2). One or more of these calibration lines need to be established for each grain mount or thin section in order to correct for variable bias in measuring $^{206}Pb^+/UO^+$ and $^{208}Pb^+/ThO^+$ in unknown monazites.

from the following equations, which assume that the inter-elemental bias is proportionally constant:

$$\left(^{206}Pb^{+}/UO^{+}\right)_{unk}/\left(^{206}Pb^{+}/UO^{+}\right)_{std} = \left(^{206}Pb/^{238}U\right)_{unk}/\left(^{206}Pb/^{238}U\right)_{std}$$

$$\left(^{208}Pb^{+}/ThO^{+}\right)_{unk}/\left(^{208}Pb^{+}/ThO^{+}\right)_{std} = \left(^{208}Pb/^{238}Th\right)_{unk}/\left(^{208}Pb/^{232}Th\right)_{std}$$

where $(^{206}Pb^{+}/UO^{+})_{std}$ and $(^{208}Pb^{+}/ThO^{+})_{std}$ are the values for the standard calculated from the linear regression calibration at the UO_2^{+}/UO^{+} of the unknown (e.g., Fig. 5), and $(^{206}Pb/^{238}U)_{std}$ and $(^{208}Pb/^{232}Th)_{std}$ are the values assumed at the concordant age of the standard (Table 2). In deriving the analytical uncertainty in $(^{206}Pb/^{238}U)_{unk}$ and $(^{208}Pb/^{232}Th)_{unk}$, both the counting error in $(^{206}Pb^{+}/UO^{+})_{unk}$ and $(^{208}Pb^{+}/ThO^{+})_{unk}$ and the 1σ uncertainty of the relevant standard calibration line are added quadratically. Although the counting statistical uncertainties in the $^{206}Pb^{+}/UO^{+}$ and $^{208}Pb^{+}/ThO^{+}$ ratios of individual spots are typically 0.1–0.4% (1σ), the standard deviation of $^{206}Pb^{+}/UO^{+}$ and $^{208}Pb^{+}/ThO^{+}$ about the regression lines is typically $\pm$1.5–2% (Fig. 5), yielding statistically poor fits that reflect the imperfection of the calibration method and possibly real age variations in the sample (see also Ireland and Gibson, 1998). The $(^{207}Pb/^{235}U)_{unk}$ is not directly measured, but calculated from the $^{207}Pb^{*}/^{206}Pb^{*}$ and isotopic composition of natural uranium.

4.3.1. Matrix effects

The corrections to the $^{206}Pb^{+}/UO^{+}$ and $^{208}Pb^{+}/ThO^{+}$ values for the unknowns are carried out under the assumption that the bias is proportionally equivalent to that of the standard under the same analytical conditions, i.e., at the same UO_2^{+}/UO^{+}. In

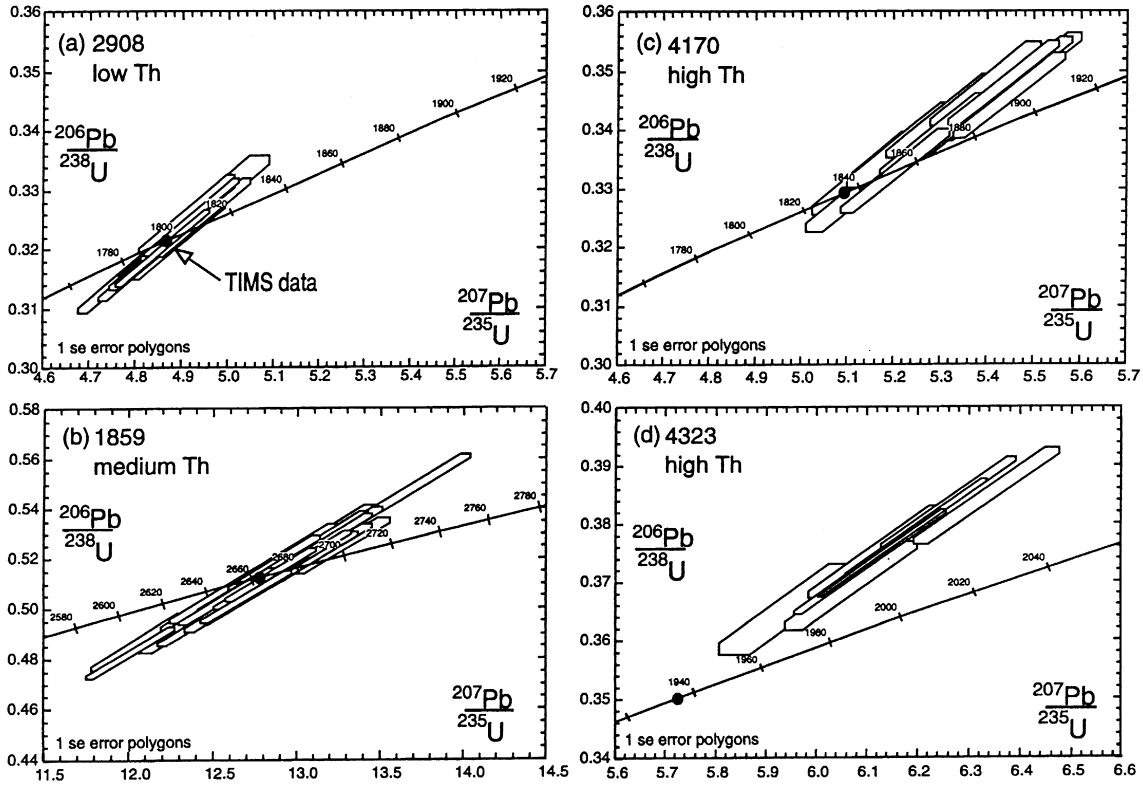

Fig. 6. U–Pb concordia plots of SHRIMP monazite data (1σ error polygons). The U/Pb ratios have been calibrated relative to monazite standard #3345 (see Fig. 5b,e). Dots show ID–TIMS ages. Note that the U/Pb calibration is effective for (a) and (b), but in (c) and (d), the SHRIMP data appear to be reversely discordant, an artifact of the U/Pb calibration (see text for discussion).

order to test whether this assumption held for the compositional range in typical natural monazites, Stern and Sanborn (1998) carried out an experiment using five of the monazite test samples, encompassing low-Th (~2 wt.%) to high-Th (~12 wt.%) types. The five samples, which included the three in-house standards (Table 2), were analyzed on a single mount, and the bias in the Pb/U and Pb/Th ratios was corrected as above by reference to a calibration curve for the medium-Th monazite 3345. The four remaining monazite samples (2908, 4170, 1859, 4323) thus constituted 'unknowns', although their concordant Pb/U and Pb/Th ages were known from ID–TIMS (Table 2).

The SHRIMP isotopic data are presented on standard Wetherill (1956) concordia plots (Fig. 6) and on Pb–U–Th concordia diagrams (Fig. 7). For the low- and medium-Th samples #2908 and #1859, the mean SHRIMP $^{206}Pb/^{238}U$ and $^{208}Pb/^{232}Th$ ages are within 0.5% of the accepted values (Fig. 6a,b; Fig. 7a,b). For these monazites, the bias was successfully removed by referencing to the 3345 standard. For the high-Th monazites (#4170, #4323), the mean SHRIMP $^{206}Pb/^{238}U$ and $^{208}Pb/^{232}Th$ ages range from 3% to 8% in excess of the TIMS data (Fig. 6c,d; Fig. 7c,d). There are no systematic differences in the mean and range of UO_2^+/UO^+ values between the high-Th samples and lower-Th samples (cf. Sircombe, 1997).

Our interpretation is that the secondary ion yields of Pb^+ from high-Th monazites are enhanced relative to low- and medium-Th monazites. Whether this effect is due to the particular experimental setup is unclear, as Sircombe (1997) found no compositionally related biases. Zhu et al. (1998), however, using moderate energy filtering and different instrumentation, found matrix effects on the $^{206}Pb/^{238}U$ ratios caused by variations in Th and/or Si contents. Crystal orientation does not appear to be a factor in monazite analysis (Sircombe, 1997).

Which compositional variables are most significant in affecting the calibrations remains to be studied, although the Th content appears to be a crucial factor. The common monazites studied here with 1–8% Th behaved similarly with respect to the secondary ion yields of Pb^+, UO^+, and ThO^+. The

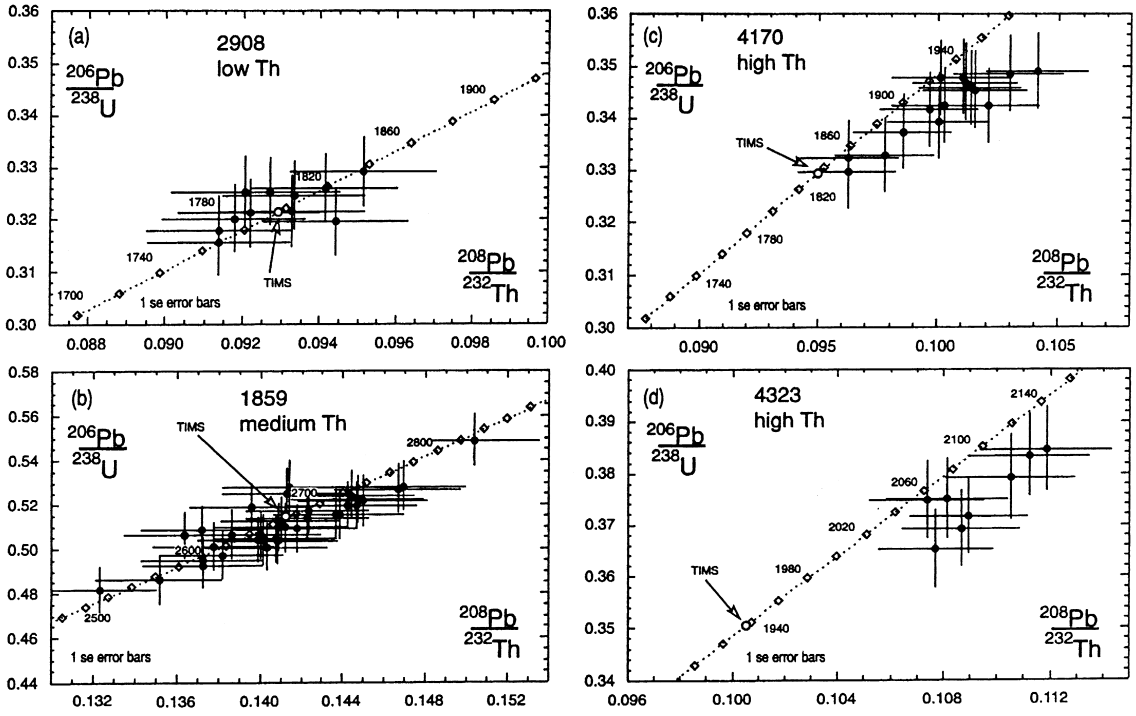

Fig. 7. U–Pb–Th concordia plots of monazite data, with U/Pb and Th/Pb ratios referenced to monazite standard #3345. As for Fig. 6, the data for high-Th monazites (c) and (d) have U–Pb and Th–Pb ages that are inaccurately high (see text for discussion).

bias in the measured Pb/U and Pb/Th ratios in these low- to medium-Th monazites was successfully removed by referencing to standards having Th contents within this range. For the high-Th monazites (> 8% Th) analyzed in our study, the residual bias in the $^{208}Pb/^{232}Th$ values was removed by referencing to a monazite #4170 with similar Th contents (Stern and Sanborn, 1998), but a residual bias of +2.5% remained in the $^{206}Pb/^{238}U$ ages. Clearly, further study of matrix effects in monazite is warranted, particularly for high-Th types (> 8 wt.%). The application in this study did not involve the analysis of high-Th monazites.

5. Part II: application of in situ monazite dating

5.1. Geological setting

The Western Churchill (WC) province is a multiply deformed and metamorphosed late Archean craton that is dominated by ca. 2.8–2.6 Ga amphibolite-grade granitoid gneisses and northeast-trending greenstone belts, and which is cut by the northeast-trending, crustal-scale deformation zone called the Snowbird tectonic zone (STZ; Fig. 8). A period of regional-scale felsic plutonism is documented at 2.58–2.62 Ga (LeCheminant and Roddick, 1991), coincident with high-grade metamorphism along the STZ (Hanmer, 1997). Paleoproterozoic events affecting the craton included deposition of intra-cratonic supracrustal rocks, and tectonic and magmatic effects associated with the bounding 2.0–1.8 Ga collisional orogens. Widespread Paleoproterozoic magmatic events included the intrusion of anorogenic granites and lamprophyre dykes at ca. 1.83 Ga, and intrusion of rapikivi granite plutons at ca. 1.75 Ga (Tella et al., 1997b; Peterson and van Breemen, 1999).

Within the Parker Lake–MacQuoid Lake region (Fig. 8), 2.68 Ga tonalite gneiss and volumetrically

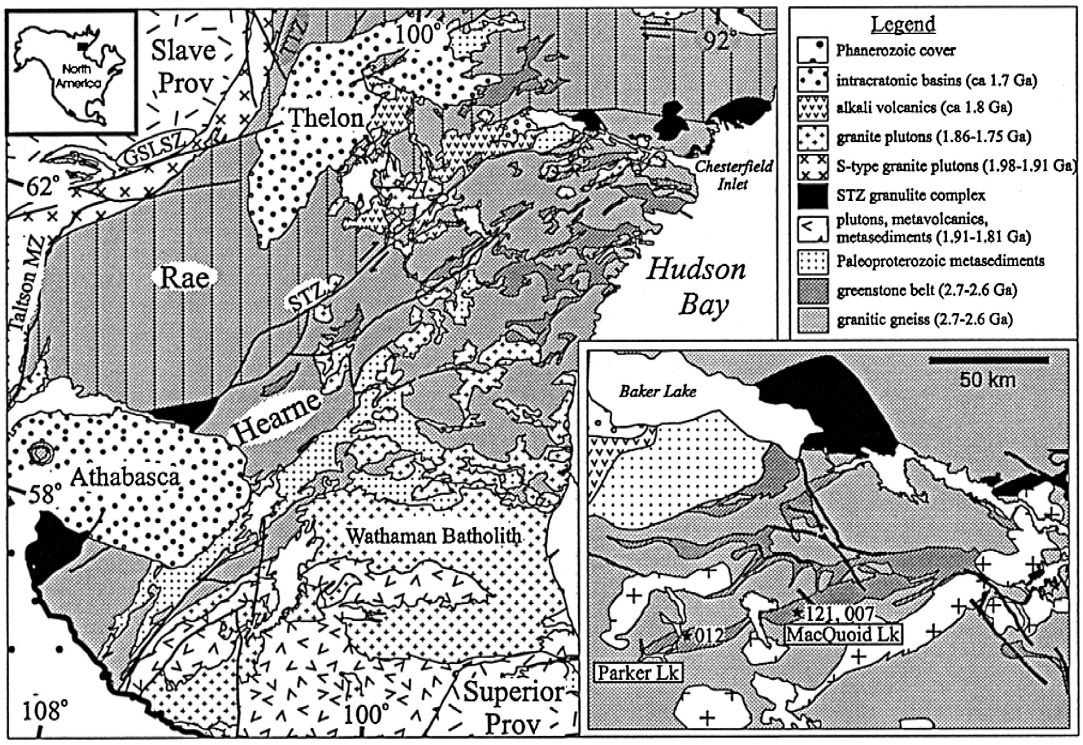

Fig. 8. Regional geology of the western Churchill province, Canadian Shield (after Hoffman, 1990). Inset shows enlarged view of the Parker Lake–MacQuoid Lake greenstone belt with the location of the study sample ('121') and others ('007', '012') discussed in the text. STZ = Snowbird tectonic zone.

minor 2.61 Ga augen granite intrude 2.75 Ga intermediate–mafic metavolcanic and psammitic–pelitic metasedimentary rocks (Tella et al., 1997a,b). The sporadic occurrence of staurolite, all three aluminosilicate polymorphs, and evidence of in situ partial melting in the metapelitic rocks, indicate that metamorphic grade ranged from lower to upper amphibolite facies. Three episodes of deformation (folding, shear zone activity) are recognized from field relations (Tella et al., 1997a,b), but the absolute ages of deformation and metamorphism are poorly constrained, especially the relative effects of late Archean vs. Paleoproterozoic events.

5.2. Sample description

Polished rock chips were studied from a whole-rock sample (96TX121) of a metapelitic unit within the greenstone belt east of Macquoid Lake. Based on field relationships, the sedimentary rock is presumed to have been deposited at about 2.75 Ga. The rock contains the assemblage Grt–Bt–St–Ms–Ky–Plg–Qz–Ap–Ilm with relict Sil (abbreviations from Kretz, 1983). Garnet porphyroblasts up to 3 cm in diameter overgrow an early S1 schistosity, but are enveloped by the main regional S2 foliation. Thin (< 0.1 mm), inclusion-laden, garnet rims overgrow the garnet porphyroblasts.

The two types of garnet are distinguished by markedly different chemistry and P–T conditions of formation. The large Grt porphyroblasts show uniform $Fe/(Fe + Mg) = 0.80–0.83$ and low CaO (< 0.036 X_{Grs}), whereas the garnet rims have elevated $Fe/(Fe + Mg) = 0.82–0.85$ and CaO (0.07–0.08 X_{Grs}). The occurrence of very similar chemical and textural features in garnet on a regional scale strongly suggests formation during two distinct metamorphic events. Thermobarometric data (Berman et al., unpublished data) yield 655°C-5.6 kbar for garnet cores, and 675°C-9.2 kbar for garnet rims.

Ion probe analyses were obtained using a 5-μm diameter primary spot from 14 (out of a total of approximately 50) monazite inclusions: three within the matrix, seven in the low-CaO garnet core, two in the high-CaO garnet rim, and two in staurolite porphyroblasts. Most monazite is 8–20 μm in diameter, except for one 40-μm inclusion within a high-CaO garnet rim. In none of the grains was any internal structure observed with BSE or cathodoluminesence imaging.

Monazite occurs in three different textural locations (A, B, F), with some variation in grain morphology in each location. Where completely armoured (monazite type 'A') by a host mineral such as low-CaO garnet or matrix plagioclase, monazite tends to form idiomorphic crystals (monazite sub-type 'Ae', armoured-euhedral; Fig. 9a) that appear to have grown in textural equilibrium with the host. Some armoured monazites, such as in the high-Ca garnet rim, display irregular outlines with many small embayments suggestive of partial resorption (monazite sub-type 'Ar') prior to incorporation into the garnet rim (Fig. 9b). Monazite grains in the matrix that are located at grain boundaries (monazite type 'B') form either subhedral to euhedral (sub-type 'Be'; Fig. 9c) grains that appear to have grown relatively late, or irregular, highly embayed crystals that appear to have been strongly resorbed (sub-type 'Br'; Fig. 9d). Other anhedral monazites with some planar faces appear to have also grown late by filling matrix interstices (sub-type 'Bi'; Fig. 9e). A third type of monazite forms irregular grains associated with late, chlorite-bearing fractures (type 'F'; Fig. 9f).

5.3. Results

U–Pb isotopic data for monazites are summarized in Table 3 and illustrated in Fig. 10. Type Ae monazites have $^{207}Pb/^{206}Pb$ ages ranging from 2499 to 2553 Ma, and are concordant to 14% discordant. Within this group, there is a crude positive correlation between age and grain size, but not with location, suggesting the possibility of diffusion-controlled Pb loss. The weighted mean $^{207}Pb/^{206}Pb$ age of the four oldest analyses from four different grains within the Ae group is 2548 ± 17 Ma, which is an estimate of the maximum age of the monazite. The type 'Ar' monazites have $^{207}Pb/^{206}Pb$ ages ranging from 2491 to 2511 Ma, and are concordant within error. Type Br monazites have $^{207}Pb/^{206}Pb$ ages ranging from 2077 to 2527 Ma, the youngest age being derived from a 7×9 μm grain partly enclosed in staurolite. Finally, three spots on a 8×60 μm type F monazite within a fracture in a high-Ca garnet rim are slightly discordant, and have a weighted

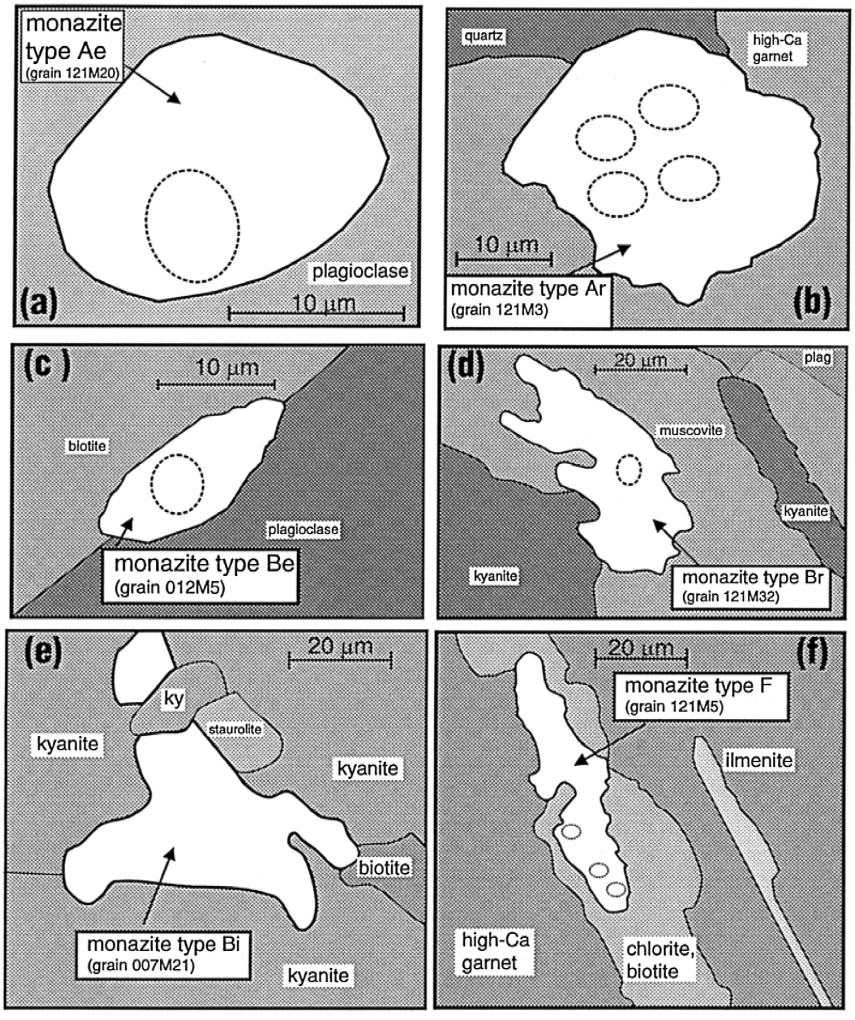

Fig. 9. Sketches of BSE reflectance images, illustrating the three basic monazite types (A: armoured; B: grain boundary; F: fracture related) and morphological subtypes (e: euhedral to subhedral; r: resorbed; i: interstitial) recognized in polished sections of metapelite samples 96TX121 (this study), 96BLB007, and 96BLB012 (Berman and Stern, unpub). Outlines of SHRIMP pits are indicated.

mean $^{207}Pb/^{206}Pb$ age of 1755 ± 30 Ma. The monazites have 1.0–3.3 wt.% Th and 632–7422 ppm U. Consistent with the SEM observations, individual grains are chemically homogeneous, and there are no consistent Chemical differences between the various types.

5.4. Interpretations

The morphology of the Ae monazite leads us to interpret the 2548 ± 17 Ma age as indirectly dating the formation of the host, low-CaO garnet. Diffusion-controlled Pb loss may explain the younger ages within this group. Some of this old monazite is also preserved within matrix plagioclase, which probably did not recrystallize at a later period. The marked contrast in CaO content between the garnet core and rim suggests that the latter grew during a younger and distinct metamorphic event, but the analyzed ca. 2.5 Ga monazite inclusion (type Ar) within the garnet rim probably represents an "inherited" grains,

which does not date this metamorphic event. These monazites appear texturally to be out of equilibrium with the rim garnet, having been partly resorbed prior to inclusion. The 2527–2078 Ma type Br monazites probably have a similar origin, and their age dispersion supports such a two-stage metamorphic history, with formation at ca. 2550 Ma followed by Pb loss and/or partial recrystallization at some later period. The maximum age of this younger event is given by the discordant 2078 Ma result for one such grain, an age that likely reflects mixing or Pb loss along a chord between ca. 2550 Ma and the age of the younger event. Although not analyzed in this specimen, type Be monazites (euhedral, grain boundary types) from other metapelitic rocks in the vicinity yield an age of ca. 1900 Ma (Berman and Stern (unpub)), suggesting that such grains grew during the younger metamorphic event, whereas the Br grains appear to be inherited from the first event. We suggest that the high-CaO garnet rims and some staurolite porphyroblasts probably crystallized at ca. 1900 Ma. The association of chlorite with the 1755 Ma, type F monazite suggests growth during greenschist facies retrograde metamorphism.

Table 3
Shrimp U/Pb monazite data for garnet metapelite 96TX121

Spot name	Mineral association	U (ppm)	Th (ppm)	Th/U	Pb (ppm)	$^{204}Pb/^{206}Pb$	$\pm^{204}Pb/^{206}Pb$	f_{206}	$^{208}Pb/^{206}Pb$
Type A (armoured)									
Sub-type e (subhedral to euhedral)									
121m-8.1	low-Ca garnet core	5224	26 651	5.1	5413	1.81e − 05	6.07e − 06	2.50e − 04	1.318
121m-9.1	low-Ca garnet core	4928	25 979	5.3	5274	3.36e − 05	3.88e − 05	4.70e − 04	1.546
121m-10.2	low-Ca garnet core	1632	33 934	20.8	4679	4.56e − 05	3.50e − 05	6.40e − 04	5.739
121m-10.4	low-Ca garnet core	729	15 087	20.7	2007	1.17e − 04	3.65e − 05	1.63e − 03	6.702
121m-10.5	low-Ca garnet core	632	11 480	18.2	1690	2.56e − 05	4.36e − 05	3.60e − 04	6.068
121m-11.1	low-Ca garnet core	1967	24 205	12.3	4028	1.73e − 06	1.56e − 05	2.00e − 05	3.669
121m-15.1	low-Ca garnet core	5619	27 427	4.9	5565	2.29e − 05	7.14e − 06	3.20e − 04	1.361
121m-15.2	low-Ca garnet core	1613	26 447	16.4	4123	2.22e − 05	2.45e − 05	3.10e − 04	4.997
121m-18.1	low-Ca garnet core	2384	24 761	10.4	4065	6.91e − 05	2.69e − 05	9.70e − 04	2.982
121m-22.1	low-Ca garnet core	6117	24 016	3.9	5834	7.71e − 06	6.49e − 06	1.10e − 04	1.131
121m-20.1	matrix plagioclase	2114	20 048	9.5	3327	3.21e − 05	2.56e − 05	4.50e − 04	2.694
121m-21.1	matrix plagioclase	1310	28 824	22.0	4122	3.79e − 05	2.65e − 05	5.30e − 04	6.565
Sub-type r (resorbed)									
121m-3.1	high-Ca garnet rim	7295	27 478	3.8	6432	1.55e − 05	1.14e − 05	2.20e − 04	1.070
121m-3.2	high-Ca garnet rim	7090	26 718	3.8	6505	1.27e − 05	1.03e − 05	1.80e − 04	1.066
121m-3.3	high-Ca garnet rim	6620	26 279	4.0	5907	7.03e − 06	5.50e − 06	1.00e − 04	1.100
121m-3.4	high-Ca garnet rim	7422	28 231	3.8	6915	8.31e − 06	9.65e − 06	1.20e − 04	1.062
Type B (grain boundary)									
Sub-type r (resorbed)									
121m-29.1	staurolite	4321	26 084	6.0	5178	9.00e − 08	1.26e − 05	0.00e + 00	1.760
121m-30.1	staurolite	2888	23 339	8.1	3236	1.10e − 04	2.08e − 05	1.64e − 03	2.547
121m-32.1	muscovite, kyanite	5998	24 362	4.1	5651	2.27e − 06	8.93e − 06	3.00e − 05	1.169
Type F (fracture-related)									
121m-5.1	high-Ca garnet rim	3155	15 331	4.9	2102	1.42e − 04	7.34e − 05	2.22e − 03	1.492
121m-5.2	high-Ca garnet rim	1901	18 002	9.5	2266	1.88e − 04	3.59e − 05	2.91e − 03	3.392
121m-5.3	high-Ca garnet rim	2416	10 466	4.3	1490	1.50e − 04	9.97e − 05	2.31e − 03	1.328

Uncertainties reported at 1σ and are calculated by numerical propagation of all known sources of error. f_{206} refers to mole fraction of total ^{206}Pb that is due to common Pb; data have been common Pb corrected according to procedures outlined in the text. Concordance = $100 \times (^{206}Pb/^{238}U \text{ age})/(^{207}Pb/^{206}Pb \text{ age})$.

5.5. Implications

Whereas previous studies have emphasized 2.58–2.62 Ga as the major period of felsic magmatism and high-grade metamorphism in the WC province (LeCheminant and Roddick, 1991; Hanmer, 1997), the in situ ion probe data point to two younger metamorphic events: a low-intermediate pressure, upper amphibolite facies event at 2548 Ma, and a greenschist facies event at 1755 Ma. The similarity of the older age to the 2560 Ma age determined for monazite within low-intermediate pressure garnet 30 km to the west at Parker Lake (Fig. 8; Berman and Stern, unpub) adds some further support to their suggestion that this event likely represents a regional-scale metamorphic event within the WC. The younger, greenschist facies metamorphism appears to be related to the intrusion over much of the western part of the WC of a high-level, ca. 1.75-Ga, rapikivi granite suite (Peterson and van Breemen, 1999). Other metapelitic rocks in the greenstone belt contain 1.9 and 1.83 Ga monazites, the former interpreted as dating high-pressure metamorphism and growth of high-CaO garnet, and the latter coinciding

$\pm^{208}Pb/^{206}Pb$	$^{206}Pb/^{238}U$	$\pm^{206}Pb/^{238}U$	$^{207}Pb/^{235}U$	$\pm^{207}Pb/^{235}U$	$^{207}Pb/^{206}Pb$	$\pm^{207}Pb/^{206}Pb$	Apparent ages (Ma)				Concordance (%)
							$^{206}Pb/^{238}U$	$\pm^{206}Pb/^{238}U$	$^{207}Pb/^{206}U$	$\pm^{207}Pb/^{206}Pb$	
0.004	0.4826	0.0091	11.02	0.21	0.1656	0.0005	2539	40	2513	5	101.0
0.023	0.4566	0.0109	10.35	0.30	0.1643	0.0022	2425	48	2501	22	97.0
0.090	0.4789	0.0232	11.00	0.55	0.1667	0.0015	2523	102	2524	15	99.9
0.029	0.4034	0.0087	9.42	0.22	0.1694	0.0012	2185	40	2552	12	85.6
0.056	0.4264	0.0086	9.83	0.22	0.1673	0.0014	2289	39	2531	14	90.5
0.018	0.4891	0.0103	11.36	0.26	0.1684	0.0010	2567	45	2542	10	101.0
0.005	0.4538	0.0088	10.27	0.21	0.1642	0.0006	2412	39	2499	6	96.5
0.023	0.4784	0.0097	11.14	0.24	0.1688	0.0010	2520	42	2546	10	99.0
0.013	0.4748	0.0099	10.79	0.24	0.1649	0.0009	2504	43	2507	9	99.9
0.005	0.4810	0.0092	10.93	0.22	0.1648	0.0007	2532	40	2506	7	101.0
0.015	0.4706	0.0112	11.00	0.28	0.1695	0.0011	2486	49	2553	11	97.4
0.030	0.4695	0.0096	10.84	0.24	0.1674	0.0010	2482	42	2532	10	98.0
0.006	0.4565	0.0088	10.41	0.21	0.1653	0.0008	2424	39	2511	8	96.5
0.007	0.4761	0.0093	10.82	0.23	0.1649	0.0009	2510	41	2506	9	100.2
0.004	0.4565	0.0087	10.28	0.21	0.1634	0.0007	2424	39	2491	7	97.3
0.007	0.4845	0.0093	11.02	0.23	0.1650	0.0009	2547	41	2507	9	101.6
0.011	0.4737	0.0092	10.90	0.22	0.1669	0.0008	2500	40	2527	8	98.9
0.010	0.3517	0.0075	6.23	0.14	0.1285	0.0006	1943	36	2078	9	93.5
0.003	0.4677	0.0087	10.53	0.20	0.1633	0.0004	2474	38	2490	4	99.4
0.021	0.2956	0.0068	4.34	0.13	0.1065	0.0018	1669	34	1740	32	96.0
0.017	0.3053	0.0068	4.55	0.12	0.1081	0.0012	1717	34	1767	20	97.2
0.027	0.3013	0.0075	4.46	0.17	0.1073	0.0027	1698	37	1754	46	96.8

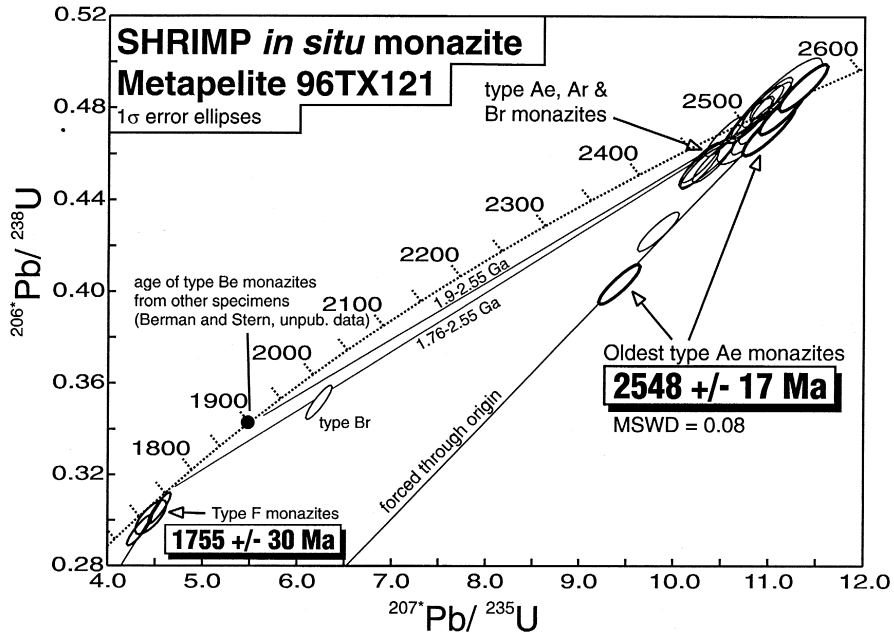

Fig. 10. U–Pb concordia diagram for monazites analyzed in situ from metapelite 96TX121. Trajectories for Pb loss or recrystallization of 2.55 Ga monazite at 1.9 and 1.76 Ga are shown. Most of the monazites are 2.50–2.55 Ga, thought to encompass the first peak metamorphic event that generated low-CaO garnet, while the fracture-related (Type F) variety is 1.76 Ga, and thought to be related to greenschist–facies retrogression. A metamorphic episode at 1.9 Ga, although not documented in this sample, is preserved in similar samples elsewhere (Berman and Stern, unpublished data).

with intrusion of a ca. 1.83-Ga anorogenic granite suite (Berman and Stern, unpublished data). Thus, on a regional scale there is evidence for growth of at least four generations of monazite formed under a range of pressure, temperature, and fluid conditions.

6. Conclusions

The analytical method of U–Pb and Th–Pb geochronology by ion microprobe as described here shows that the level of precision and accuracy is comparable to that attainable with zircon. Nevertheless, there are two specific areas where accuracy could be compromised in an ion microprobe study of monazite. Firstly, the presence of an interfering isobar at mass 204 that was suspected by previous workers has been confirmed, although the ionic species is not identified. The intensity of the isobar is positively correlated with the Th content of the monazite, and if unrecognized, its presence could cause the $^{207}Pb^{*}/^{206}Pb^{*}$ ages to be biased low by as much as several percent when corrected for common Pb using the measured $^{204}Pb^{+}$. Recognition of the 204 isobar can be made using the techniques described herein, although only data having $^{204}Pb^{+}/^{206}Pb^{+} > 0.0001$ would be sufficiently affected by the isobar to warrant attention. A small positive energy offset appears to eliminate the isobar from an analysis, but at significant reduction of the secondary ion count rates.

Secondly, there exists a compositional dependence of the secondary ion yields of Pb^{+} relative to UO^{+} and ThO^{+}. The Th content of the monazite appears to be a relatively good indicator of the state of the composition (cf. Zhu et al., 1998), but there is a need for a systematic study of the compositional and/or structural variables that control monazite secondary ion yields. The matrix dependence appears to remain through moderate energy offsets (Zhu et al., 1998), and consequently, it should be considered

as a potentially significant factor regardless of the instrumental setup. Matrix matching appears to be less important for monazites with Th contents of 1–8 wt.% than for monazites with greater Th abundances.

The example application of the technique to in situ dating of 10–30 μm monazites hosted within an Archean metapelite demonstrates the benefit of the method in elucidating the origin of polyphase metamorphic rocks. Both the contextual setting and the morphology of the monazite grains provide constraints on interpreting the timing of growth of the host metamorphic mineral (e.g., garnet, staurolite, plagioclase). Whether or not the monazites appear to be in textural equilibrium seems to be an important factor in interpreting the isotopic ages as syn-genetic or inherited. Although there was little age or compositional heterogeneity evident within individual grains, there were substantial differences in the isotopic ages between individual grains. Growth of monazite occurred at 2.55 and 1.76 Ga, corresponding with high-grade and low-grade metamorphic events, respectively, that have regional geological significance.

Acknowledgements

Critical reviews of the manuscript were carried out by T. Ireland, K. MacLachlan, K. Sircombe, and M. Whitehouse, who are thanked for their many constructive suggestions. GSC Contribution No. 1999156.

References

Bethune, K., Scammell, R.J., 1997. Precambrian geology, Koch Island area (part of NTS 37C, District of Franklin, Northwest Territories). Geol. Surv. Can., Open File 3391.

Corriveau, L., van Breemen, O., Morin, D., Amelin, Y., Rivard, B., Sharma, K.N.M., 1996. New light on the Central Metasedimentary Belt of Quebec and its lithosphere. Rapp. Transect LITHOPROBE Abitibi-Grenville 49, 23–27.

Cumming, G.L., Richards, J.R., 1975. Ore lead in a continuously changing Earth. Earth Planet. Sci. Lett. 28, 155–171.

Davis, W.J., Parrish, R.R., McNicoll, V.J., Bellerive, D., 1998. Analytical procedures for the determination of 232Th/208Pb ages in the geochronology laboratory, Geological Survey of Canada. Radiogenic Age and Isotopic Studies: Report 11. Geol. Surv. Can., Curr. Res. pp. 19–22, 1998-F.

De Laeter, J.R., Kennedy, A.K., 1998. A double focusing mass spectrometer for geochronology. Int. J. Mass Spectrom. 178, 43–50.

DeWolf, C.P., Belshaw, O'Nions, R.K., 1993. A metamorphic history from micron-scale $^{207}Pb/^{206}Pb$ chronometry of Archean monazite. Earth Planet. Sci. Lett. 120, 207–220.

Grove, M., Harrison, T.M., 1999. Monazite Th–Pb age depth profiling. Geology 27, 487–490.

Hanmer, S., 1997. Geology of the Striding–Athabasca mylonite zone, northern Saskatchewan and southeastern District of Mackenzie, N.W.T. Geol. Surv. Can., Bull. 501, 92 pp.

Harrison, T.M., McKeegan, K.D., LeFort, P., 1995. Detection of inherited monazite in the Manaslu leucogranite by $^{208}Pb/^{232}Th$ ion microprobe dating: crystallization age and tectonic implications. Earth Planet. Sci. Lett. 133, 271–282.

Hoffman, P.F., 1990. Subdivision of the Churchill Province and extent of the Trans-Hudson Orogen. In: Lewry, J.F., Stauffer, M.R. (Eds.), The Early Proterozoic Trans-Hudson Orogen of North America. Geol. Assoc. Can., Spec. Pap., vol. 37, pp. 15–39.

Hogarth, D.D., van Breemen, O., 1996. Geology and age of the Lac a la Perdrix fenite, southern Gatineau district, Quebec. Radiogenic Age and Isotopic Studies: Report 9. Geol. Surv. Can., Curr. Res. pp. 33–41, 1995-F.

Ireland, T.R., Gibson, G.M., 1998. SHRIMP monazite and zircon geochronology of high-grade metamorphism in New Zealand. J. Metamorph. Geol. 16, 149–167.

Kretz, R., 1983. Symbols for rock-forming minerals. Am. Mineral. 68, 277–279.

LeCheminant, A.N., Roddick, J.C., 1991. U–Pb evidence for widespread 2.6 Ga felsic magmatism in the central District of Keewatin, N.W.T. Radiogenic Age and Isotopic Studies: Report 4. Geol. Surv. Can. pp. 91–99, Paper 90-2.

Parrish, R.R., Roddick, J.C., Loveridge, W.D., Sullivan, R.W., 1987. Uranium–lead analytical techniques at the geochronology laboratory, Geological Survey of Canada. Radiogenic Age and Isotopic Studies: Report 1. Geol. Surv. Can. pp. 3–7, Paper 87-2.

Percival, J.A., Mortensen, J.K., Stern, R.A., Card, K.D., Begin, N.J., 1992. Giant granulite terranes of northeastern Superior Province: the Ashuanipi Complex and Minto Block. Can. J. Earth Sci. 29, 2287–2308.

Peterson, T.D., van Breemen, O., 1999. Review and progress report of Proterozoic granitoid rocks of the western Churchill Province, Northwest Territories (Nunavut). Geol. Surv. Can., Curr. Res. 119–127, 1999-C.

Sircombe, K., 1997. Detrital mineral SHRIMP geochronology and provenance analysis of sediments in eastern Australia. Unpublished PhD Thesis, The Australian National University, 411 pp.

Sircombe, K., Compston, W., 1994. SHRIMP analysis of monazite and application for provenance studies. Geol. Soc. Aust. Abstr. 37, 409.

Steiger, R.H., Jäger, E., 1977. Subcommission on geochronology: convention on the use of decay constants in geo- and cosmochronology. Earth Planet. Sci. Lett. 36, 359–362.

Stern, R.A., 1996. A SHRIMP II ion microprobe at the Geological Survey of Canada. Geosci. Can. 23, 73–76.

Stern, R.A., 1997. The GSC sensitive high resolution ion microprobe (SHRIMP): analytical techniques of zircon U–Th–Pb age determinations and performance evaluation. Radiogenic Age and Isotopic Studies: Report 10. Geol. Surv. Can., Curr. Res. pp. 1–31, 1997-F.

Stern, R.A., 1998. High-resolution SIMS determination of radiogenic tracer-isotope ratios in minerals. In: Cabri, L.J., Vaughan, D.J. (Eds.), Modern Approaches to Ore and Environmental Mineralogy. Miner. Assoc. Can. 27, pp. 241–268, Short Course Series.

Stern, R.A., Sanborn, N., 1998. Monazite U–Pb and Th–Pb geochronology by high-resolution secondary ion mass spectrometry. Radiogenic Age and Isotopic Studies: Report 11. Geol. Surv. Can., Curr. Res. pp. 1–18, 1998-F.

Tella, S., Davis, W., Berman, R.G., Stern, R., Lecheminant, A.N., 1997a. Tectonothermal history of the MacQuoid Lake supracrustal belt, District of Keewatin, Northwest Territories, Canada. Geol. Soc. Am. Abstr. Prog. 29, A277.

Tella, S., LeCheminant, A.N., Sanborn-Barrie, M., Venance, K.E., 1997b. Geology and structure of parts of MacQuoid lake map area, District of Keewatin, Northwest Territories, Canadian Shield. Geol. Surv. Can., Curr. Res. 123–132, 1997-C.

Vry, J., Compston, W., Cartwright, I., 1996. SHRIMP II dating of zircons and monazites: reassessing the timing of high-grade metamorphism and fluid flow in the Reynolds Range, northern Arunta Block, Australia. J. Metamorph. Geol. 14, 335–350.

Wetherill, G.W., 1956. Discordant uranium–lead ages. Trans. Am. Geophys. Union 37, 320–326.

Williams, I.S., 1998. U–Th–Pb geochronology by ion microprobe. In: McKibben, M.A., Shanks, W.C., Ridley, W.I. (Eds.), Applications of Microanalytical Techniques to Understanding Mineralizing Processes. Rev. Econ. Geol., vol. 7, pp. 1–35.

Williams, I.S., Buick, I.S., Cartwright, I., 1996. An extended episode of early Mesoproterozoic metamorphic fluid flow in the Reynolds Range, central Australia. J. Metamorph. Geol. 14, 29–47.

Wodicka, N., Scott, D.J., 1997. A preliminary report on the U–Pb geochronology of the Meta Incognita Peninsula, southern Baffin Island, Northwest Territories. Geol. Surv. Can., Curr. Res. 167–178, 1997-C.

Zhu, X.K., O'Nions, R.K., Belshaw, N.S., Gibb, A.J., 1997a. Lewisian crustal history from in situ SIMS mineral chronometry and related metamorphic textures. Chem. Geol. 136, 205–218.

Zhu, X.K., O'Nions, R.K., Belshaw, N.S., Gibb, A.J., 1997b. Significance of in situ SIMS chronometry of zoned monazite from the Lewisian granulites, northwest Scotland. Chem. Geol. 135, 35–53.

Zhu, X.K., O'Nions, R.K., Gibb, A.J., 1998. SIMS analysis of U–Pb isotopes in monazite: matrix effects. Chem. Geol. 144, 305–312.

Zhu, X.K., O'Nions, R.K., 1999. Zonation of monazite in metamorphic rocks and its implications for high temperature thermochronology: a case study from the Lewisian terrain. Earth Planet. Sci. Lett. 171, 209–220.